

# FINAL PUBLISHABLE REPORT

Grant Agreement number 14IND01  
 Project short name 3DMetChemIT  
 Project full title Advanced 3D chemical metrology for innovative technologies

Project start date and duration:		01 June 2015, 36 months
Coordinator: Rasmus Havelund, NPL Tel: +44 208 943 6202 E-mail: <a href="mailto:rasmus.havelund@npl.co.uk">rasmus.havelund@npl.co.uk</a>		
Project website address: <a href="http://empir.npl.co.uk/3dmetchemit/">http://empir.npl.co.uk/3dmetchemit/</a>		
Internal Funded Partners: Partner 1 NPL, United Kingdom Partner 2 CEA, France Partner 3 CMI, Czech Republic Partner 4 INRIM, Italy Partner 5 PTB, Germany	External Funded Partners: Partner 6 CNR, Italy Partner 7 FCT-UNL, Portugal Partner 8 IMEC, Belgium Partner 9 UPO, Italy Partner 10 UNOTT, United Kingdom	Unfunded Partners: Partner 11 CPI, United Kingdom Partner 12 ION-TOF, Germany

**Report Status: PU Public**

Final Publishable Report

*This publication reflects only the author's view and the Commission is not responsible for any use that may be made of the information it contains.*



The EMPIR initiative is co-funded by the European Union's Horizon 2020 research and innovation programme and the EMPIR Participating States

**TABLE OF CONTENTS**

1	Overview .....	3
2	Need .....	3
3	Objectives .....	3
4	Results .....	4
4.1	Objective 1 .....	4
4.2	Objective 2 .....	9
4.3	Objective 3 .....	14
4.4	Objective 4 .....	16
5	Impact .....	25
6	List of publications .....	26

## 1 Overview

European industry and manufacturing had a need for improved capability for 3D-resolved chemical composition and interfacial material properties measurement. This project advanced the measurement capability and developed trusted measurement procedures for 3D chemical imaging at the micro- and nano-scale. Prototype instrumentation is now available and accessed by industry at consortium partner organisations using the developed procedures.

## 2 Need

Prior to the start of the project there was a need for improved chemical imaging in 3D. The need was, and still is, driven by the incessant demands from consumers for innovation in high value-added manufacturing. To meet the demands, industry had increasingly turned to the use of 3D architectures, additive manufacturing and a rapidly expanding library of materials. This was equally the case for devices based on organic materials, such as smart optical films and advanced coatings, as it was for inorganic nano-layered, high-density 3D devices. In many technologies, e.g. sensors and semiconductors, the interface between organic and inorganic materials caused severe measurement issues. This created the need for beyond state-of-the-art capabilities to measure chemical composition and interfacial properties with 3D-spatial resolution.

A major issue for organic multi-layer technologies and coatings, such as light management films are inclusions leading to defects at buried interfaces. The state of the art for industrial analysis of buried interfaces at the start of the project relied on cross-sectioning with a microtome, which is often unsuccessful as it is a 'hit and miss' affair. 3D chemical imaging, based on ion beam etching in combination with layer-by-layer imaging was identified as a promising technique for revealing and identifying defects in 3D, but lacked the required capability for chemical identification and failed for heterogeneous devices where the ion beam etching rate varies within the material.

In the semiconductor, steel and energy storage industries, analysts are faced with challenges to measure the chemical composition of inorganic devices or heterogeneous systems containing organic/inorganic layers and interfaces. A notorious example is the need to measure dopants in next-generation semiconductor devices in 3D on the sub-nm scale. The combination of 3D-spatial resolution (< nm), mass identification (isotope selectivity) and sensitivity (< 10 ppm) made atom probe tomography (APT) a major contender for these characterisation needs. However, as an emerging technology, APT had many artefacts, it completely lacked standardisation, and insights into the fundamental physics underpinning its technology were lacking.

## 3 Objectives

The overall aim of the project was to provide European industry and manufacturing with urgently needed, trusted measurement capability and standards for 3D-resolved chemical composition and interfacial material properties.

The project addressed the following scientific and technical objectives:

1. To develop metrology for chemical and compositional 3D imaging of organic and heterogeneous devices with high mass resolution chemical identification (> 100 000) and sub-micron spatial resolution (80 nm) using mass spectrometry.
2. To develop metrology for reliable and traceable detection, identification, localisation and quantification of chemical components in the depth of organic layers to improve accuracy and achieve sub-50 nm resolution in 3D chemical imaging by resolution enhancement resulting from the integration of topography information in the 3D reconstruction of chemical data.
3. To develop metrology for atomic resolution 3D elemental imaging techniques for inorganic devices and improvement of tomographic methods. The objective is to obtain layer thickness/quantification accuracy better than 5 % and repeatability better than 20 % in heterogeneous systems where distortions are known to occur at present.
4. To develop a metrological traceable method for quantifying element depth profiles in 3D structured nano-layered devices and 3D nano-structured reference materials with a high control of shape and size using

organic domain structures ranging from 10 nm to 100 nm, to transfer traceability to online analytical instrumentation.

5. To engage with industry to facilitate the take up of the technology and measurement infrastructure developed by the project, to support the development of new, innovative products and thereby enhance the competitiveness of EU industry.

## 4 Results

This section gives an account of the project's outputs delivered against each of the project's objectives.

### 4.1 Objective 1

*To develop measurement techniques for chemical and compositional 3D imaging of organic and heterogeneous devices with high-resolution chemical identification of phase separated and buried domains with a mass resolution of > 100 000 and sampling from sub-micron areas (80 nm).*

#### High mass resolving power SIMS imaging

Secondary ion mass spectrometry (SIMS) has become a powerful tool for label-free chemical imaging with high spatial resolution. The technique is based on the process of sputtering in which the sample is bombarded with energetic ions that desorb material from the sample surface. Some of the desorbed molecules and molecular fragments are charged and can be analysed using a mass analyser. During the past three decades, the emergence of new cluster ion sources has led to new capabilities for the analysis of organic samples using SIMS. A major step forward came with the introduction of gas cluster ion sources which has made depth profiling and 3D imaging of a wide range of organic materials and devices possible. SIMS is now used for the analysis of e.g. organic electronic devices, medical devices, and biological samples.

However, the state of the art in SIMS instrumentation at the outset of this project had critical limitations for the analysis of complex organic samples. SIMS instruments used for analysis of organic materials typically use time-of-flight mass analysers (ToF-SIMS) which have insufficient mass resolving power and mass accuracy to distinguish different chemical groups with nearly the same mass. Chemical identification with these analysers is in general based on prior knowledge of the sample and libraries of mass spectra from common materials. A new instrument called the 3D OrbiSIMS brings developments in mass analyser technology to SIMS in order to achieve a 30-fold improvement in mass resolving power in SIMS ( $m/\Delta m$ ) from 10 000-15 000 to > 400 000. This significantly improves the certainty with which chemical constituents can be identified. In brief, the instrument, built by consortium member ION-TOF GmbH, Germany, incorporates a Thermo Fischer Scientific QExactive HF mass spectrometer with an Orbitrap™ mass analyser in a state-of-the-art ToF-SIMS instrument. It is equipped with a gas cluster ion beam (GCIB) with an optimal focus better than 2 μm and liquid metal ion source for imaging with a lateral resolution down to 80 nm. The dual-beam dual-analyser configuration gives unprecedented 3D chemical imaging capability. In the 3DMetChemIT project, the instrument capabilities have been assessed and metrology has been developed to exploit the instrument to meet industry requirements for spatially resolved chemical analysis by the National Physical Laboratory (NPL, UK) and ION-TOF.

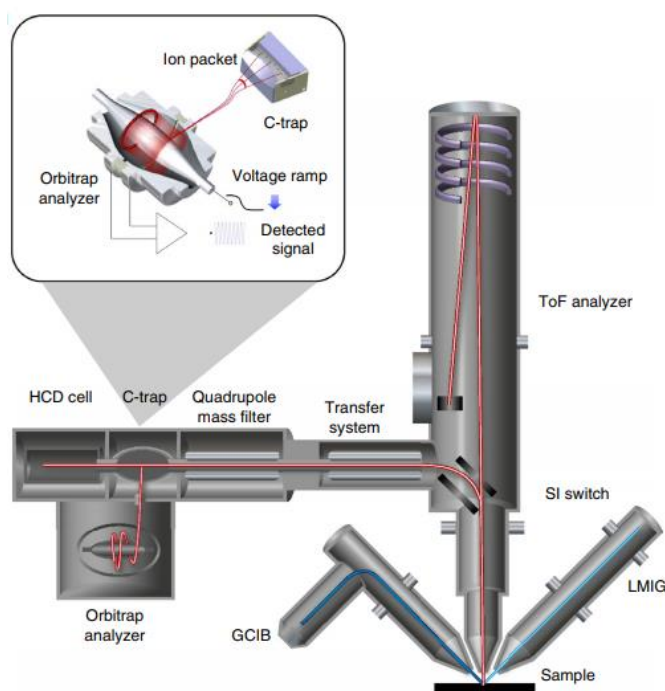


Figure 1: Schematic of the 3D OrbiSIMS.

The mass resolving power using the Orbitrap mass analyser depends on the scan time set for the Orbitrap analyser and can exceed 480 000. To demonstrate nanoscale resolution using the Bi LMIG simultaneously with high mass resolution using the Orbitrap MS, a sample of zirconium dioxide ( $\text{ZrO}_2$ ) nanostructures was imaged using a highly focused  $\text{Bi}_3^{++}$  beam and analysing with the Orbitrap mass analyser which gave a mass-resolving power of 355 000 at  $m/z$  105.8991. The lateral resolution, evaluated on  $\text{ZrO}_2$  nanostructure edges, was found to be  $172 \text{ nm} \pm 61 \text{ nm}$ .

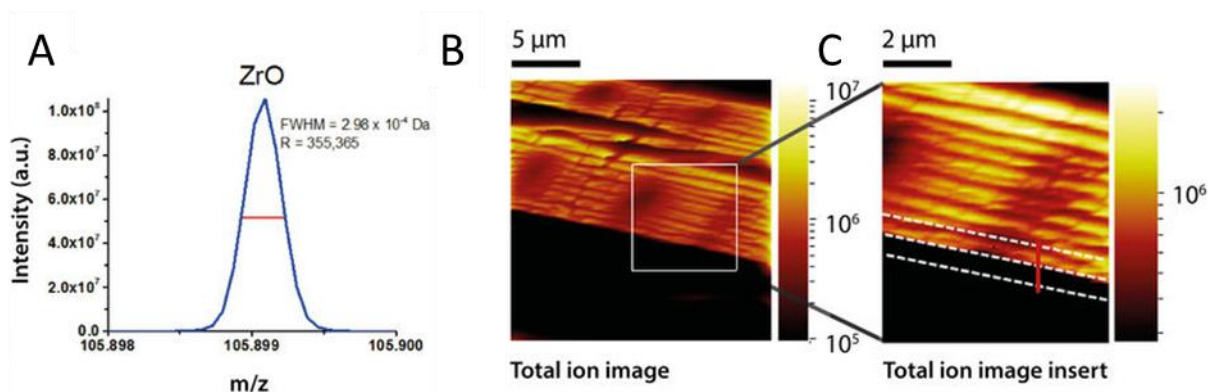


Figure 2: A) The  $[\text{ZrO}]^+$  peak at  $m/z$  105.8991 (0.2 ppm) with a FWHM width of 0.3 mDa and mass resolving power of 355 000. B) Total ion images of  $\text{ZrO}_2$  crystals obtained with the Bi LMIG source with insert, C) showing detail of thin nanostructures. The lateral resolution was evaluated for linescans obtained along the  $y$ -axis of the ion image across the  $\text{ZrO}_2$  crystal edge.

A key challenge which was targeted in the 3DMetChemIT project is the analysis of buried domains. SIMS depth profiling and 3D imaging using argon cluster sputtering offers the ability to analyse buried layers in organic materials. In most ToF-SIMS instruments this is achieved in a dual-beam mode where, typically, a

crater is formed using an Ar cluster ion beam, e.g.  $\text{Ar}_{2000}^+$ , and the bottom of the crater formed by the Ar cluster beam is imaged using a  $\text{Bi}_3$  or  $\text{Au}_3$  primary ion beam. A drawback of this method is that all the material that is eroded by the Ar cluster beam does not contribute analytical information as a continuous stream of ions cannot directly be analysed with a ToF mass analyser. This, however, is possible using the Orbitrap mass analyser. In the 3D OrbiSIMS this is exploited in different modes of operation where the Orbitrap mass analyser analyses the material sputtered by the gas cluster ion beam and, if required, images are obtained using a  $\text{Bi}_3^+$  beam and analysing the secondary ions generated by that beam with the ToF mass analyser. The need for the  $\text{Bi}_3/\text{ToF}$  analyser combination is two-fold. 1) The Orbitrap mass analyser's scan rate is slow and hence, high resolution imaging can take several hours for a single scan. 2) The optimal beam focus achievable with the gas cluster ion beam gives a lateral resolution just under  $2\ \mu\text{m}$ . With  $\text{Bi}_3$  lateral resolutions below 200 nm, or even 100 nm, are achievable.

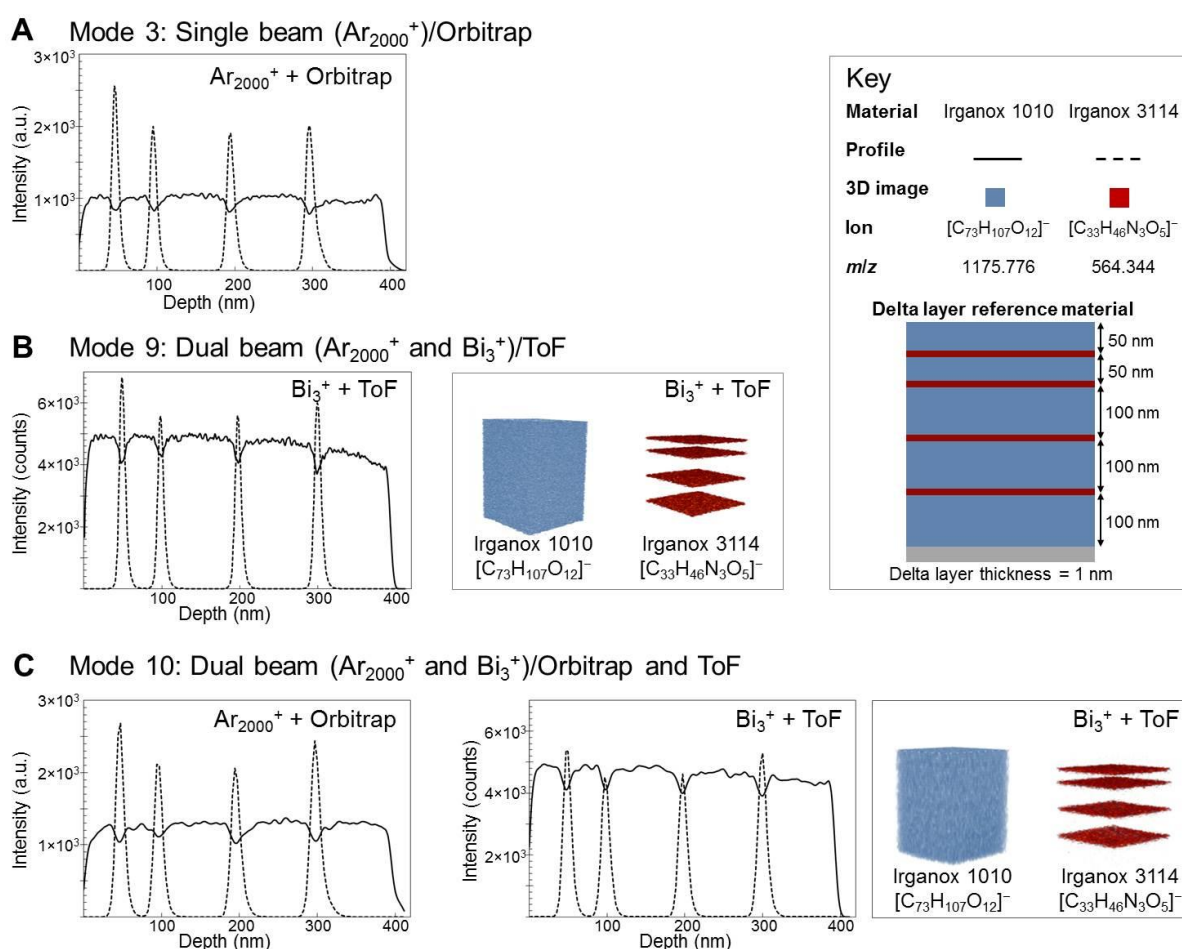


Figure 3: A) Orbitrap MS (mode 3), 5 keV  $\text{Ar}_{2000}^+$  sputtering and analysis, intensity depth profile of the Irganox 1010 molecular ion,  $[\text{C}_{73}\text{H}_{107}\text{O}_{12}]^-$  at *m/z* 1175.776 (solid line), and fragment ion from Irganox 3114,  $[\text{C}_{33}\text{H}_{46}\text{N}_3\text{O}_5]^-$  at *m/z* 564.344 (dashed line). B) ToF MS (mode 9), 5 keV  $\text{Ar}_{2000}^+$  sputtering and 30 keV  $\text{Bi}_3^+$  analysis intensity depth profile, as A) with 3D reconstruction from ToF MS data and C) Dual analyser, dual beam mode (10) with 5 keV  $\text{Ar}_{2000}^+$  sputter beam. Intensity depth profiles as A) for Orbitrap MS  $\text{Ar}_{2000}^+$  analysis beam and ToF MS 30 keV  $\text{Bi}_3^+$  beam, with 3D reconstruction from ToF MS data.

In the 3DMetChemIT project, the ability to perform analysis of buried domains was assessed using an existing NPL organic multilayer test material. This material consists of a 400 nm thick film of the organic compound Irganox 1010. Embedded in the film are thin layers of a different organic compound, Irganox 3114, at 50 nm, 100 nm, 200 nm, and 300 nm depth. Depth profiles and 3D images were obtained from the test material using the modes described above. The results are shown in Figure 3. The depth resolution achieved across all

modes was around 10 nm. The profiles show a good dynamic range at the Irganox 3114 layers of at least three orders of magnitude. This would indicate sensitivity to concentrations to the 10s of ppm. A comparable measurement of the sensitivity was done a set of polymer films made from mixtures of polystyrene with deuterated polystyrene. The deuterated material was detected at 0.01 wt % concentration. The sensitivity was also evaluated from spectra obtained from only a small amount of material where it was found that an amount of 10 fmol of Irganox 1010 is sufficient to generate a spectrum that permits its detection.

The Centre for Process Innovation (CPI, UK) prepared organic light emitting diodes (OLEDs) for evaluation of the 3D OrbiSIMS instrument's capability for this important class of devices. Organic electronics devices are becoming increasingly important but the development of organic electronic devices poses a number of scientific and technological challenges related to their large scale processing and manufacture, efficiency, and stability. Metrology that permits accurate and quantitative measurements of chemistry at the nanoscale is essential for addressing these challenges. Its excellent depth resolution and high sensitivity make secondary ion mass spectrometry (SIMS) with gas cluster ion beam sputtering a powerful capability for analysing organic electronic devices. The 3D OrbiSIMS further brings the benefit of high mass-resolving power. This was required for the green OLED devices provided by CPI where the Orbitrap mass analyser resolved secondary ions from two different materials in a mixed layer as separate peaks. The separate ions were not fully resolved in ToF spectra.

The high mass-resolving power and excellent mass accuracy provided by the Orbitrap mass analyser greatly improves the certainty with which secondary ion assignments can be made to peaks in the SIMS spectra so that chemical components in the samples can be identified. However, the position of a peak in a spectrum is often not sufficient for unambiguous identification. In those cases, tandem mass spectrometry provides valuable structural information. The ability to perform tandem mass spectrometry at buried domains using the Q Exactive mass spectrometer was demonstrated and evaluated in the 3DMetChemIT project. To further support chemical information, a novel fast algorithm was developed for identifying chemical species in the mass spectrum. The algorithm searches available databases for potential chemical annotations and reduces the large number of candidates by retaining only those that are correlated to isotope distributions of the given mass. This provides a method for fast molecular identification that removes unlikely molecules. Although not currently integrated in to an online set up, this algorithm could be integrated with an instrument to search spectra in near real time.

The above results from the 3DMetChemIT project shows the achieved performance of the 3D OrbiSIMS instrument in terms of mass resolving power and lateral resolution. Imaging with a mass-resolving power > 300 000 with a simultaneous lateral resolution of 172 nm is an astounding result. A lateral resolution of < 80 nm was targeted, and whilst it is possible to focus the Bi beam to spot sizes smaller than 80 nm, the erosion of the sample during data acquisition limits the effective spatial resolution. Any further improvement of the lateral resolution would require higher sensitivity so that a smaller volume of material would need analysing for an image to be obtained. The lower resolution achieved is considered satisfactory.

#### SIMS imaging of heterogeneous devices

A second part of Objective 1 was to develop methods for the analysis of heterogeneous materials and devices. The growing interest in hybrid organic-inorganic devices and materials, e.g. composites, creates a need for methods for their characterisation. However, 3D SIMS analysis of such materials is usually difficult since the different phases sputter very differently. A GCIB is virtually unable to sputter inorganics. An alternative approach is to use focused ion beam (FIB) milling to mill away material and expose buried interfaces for high-resolution SIMS imaging. This was investigated in the 3DmetChemIT project by NPL and ION-TOF.

A test device based on a microchannel plate consisting of a regular honeycomb array of tubes of 10  $\mu\text{m}$  diameter in glass was developed. The tubes were filled with polystyrene (PS) or polymethyl-methacrylate (PMMA) by melting the polymers and pressing them into the tubes in a vacuum oven. This regular structure of organic and inorganic phases was used for evaluating the lateral resolution, the organic material damage effects and the data validity. A Ga FIB was used for the milling of the test is able to mill both inorganic and organic materials but the milled organic phases are severely damaged in the near surface region (< 10 nm from the surface). It was shown that the damage can be removed using a GCIB to recover molecular ion signals from the organic phases. The use of a GCIB clean-up cycle had not reported before the project started and a

systematic study was required. Using the test device, we determined that clean-up using 10 keV  $\text{Ar}_{2500}^+$  doses of 10 ions/ $\text{nm}^2$  and 60 ions/ $\text{nm}^2$  are required to recover the organic signal for PMMA and PS respectively.

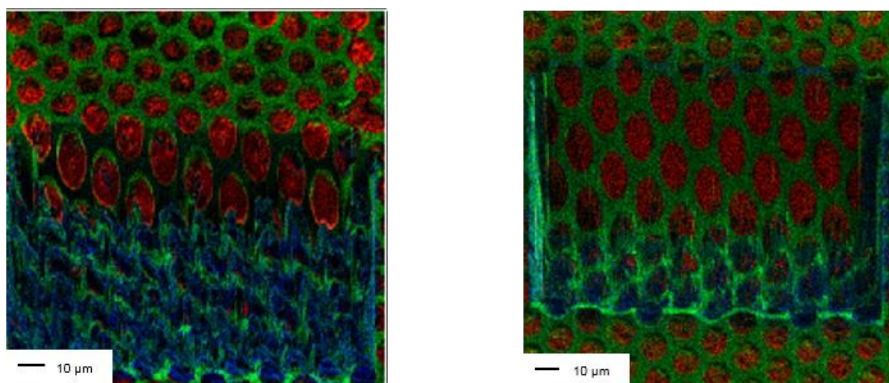


Figure 4: Secondary ions image overlays of inorganic signal coming from MCP test device as Rb in green, Ga in blue with the organic signal in red coming from the characteristic fragments, respectively, as  $\text{C}_7\text{H}_7^+$  for PS (left) and  $\text{C}_4\text{H}_5\text{O}^+$  for PMMA (right). The images have been obtained after GCIB clean-up.

We postulated that since  $\text{Bi}_3^+$  has a higher sputtering yield than  $\text{Ga}^+$  for organics, that the effects of damage on organics could be less. We used the test-device to evaluate this for FIB milling with 30 keV  $\text{Ga}^+$ ,  $\text{Bi}^+$  and  $\text{Bi}_3^+$ . We found, the reverse is in fact the case and have explained this in terms of a theory based on the angular dependent sputtering yield. In this theory, the angle of incidence evolves from the initial  $45^\circ$  geometrical angle with the fresh surface to stabilise at near  $\theta_{\text{max}}$  as the milling proceeds. Since  $\theta_{\text{max}}$  differs substantially between atomic (approximately grazing) and cluster projectiles (approximately  $45^\circ$ ) then the ability to successfully mill through materials with vastly different sputtering rates is affected. Therefore, gallium is recommended for milling organic-inorganic hybrid materials.

The optimised methodology for analysis of heterogeneous devices was applied to analyse 3D-printed materials developed by the University of Nottingham (UNOTT, UK). Additive manufacturing is at heart an interface problem where multiple layers of material are consecutively deposited to build up a physical 3D object. For future 3D-printed electronics, co-deposition of both organic materials alongside conductive inorganics is required, resulting in complex organic-inorganic interfaces. We imaged the buried organic-inorganic interface of a 3D printed strain sensor containing a layer of silver between layers of polymer. Figure 5 shows secondary ion images of the FIB crater in the device after GCIB cleaning with a dose of 20 ions/ $\text{nm}^2$ . After removal of the implanted gallium, the interface between the two materials is clearly distinguishable. Inspection of the data, show small quantities of Ag above the silver-polymer interface. This could be interpreted as atomic diffusion whilst the overlayers are deposited or it could be from very small particles of Ag.

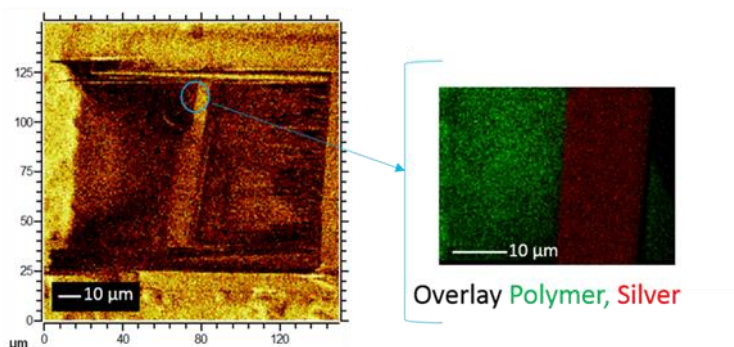


Figure 5: FIB-TOF-SIMS analysis of an additive manufactured encapsulated strain sensor. Left: total secondary ion image of milled and cleaned crater. Right: high-resolution secondary ion image of the interface with characteristic polymer fragment  $m/z$  51 (green) and silver (the sum of  $\text{Ag}_3$  and  $\text{Ag}_5$ ) (red).

A method for the preparation of cross-sections of purely organic materials such as polymer multilayer films was also developed. The method uses a high dose of gallium from a focused ion beam to produce a damaged overlayer on the surface of the organic sample. The damaged layer has a significantly slower sputter rate compared to the native undamaged organic material. Therefore, during gas cluster ion beam (GCIB) depth profiling experiments the damaged layer functions as a mask, protecting the sample beneath and producing a cross-section at the edge of the mask. As above, the FIB itself cannot be used directly to prepare the cross-section since the organic materials are easily damaged. A four step workflow was developed including a final cleaning procedure to remove redeposited material from the cross-section. The workflow can be completed in a few hours for samples up to 100  $\mu\text{m}$  thickness.

The objective of developing methods for chemical imaging of heterogeneous devices was met with the above outcomes. The detailed study of parameters related for the preparation of cross sections of inorganic-organic test devices resulted in very useful recommendations for the analysis of heterogeneous devices. For organic materials, the new in situ method may prove useful in industry as the method does not require sample embedding and is suited to automated analysis, which can be important benefits for industrial analysis where a variety of samples are analysed routinely.

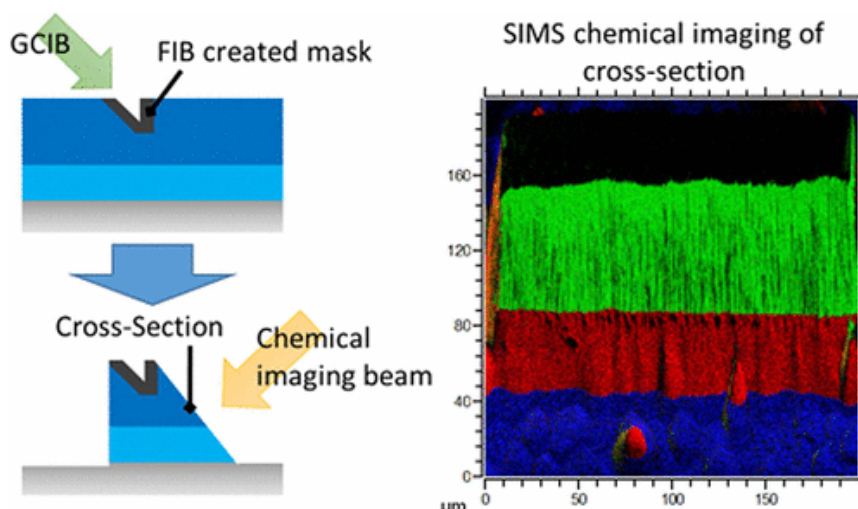


Figure 6: Overview of in situ mask preparation and cross section formation using a GCIB (left). The SIMS image to the right has been obtained from a sample of Scotch tape. Overlaid ion images are for the carrier layer  $\text{C}_2\text{H}_3\text{O}^+$  (green), for the sticky layer  $\text{C}_4\text{H}_9^+$  (red), and for the PET substrate  $\text{C}_7\text{H}_4\text{O}^+$  (blue).

## 4.2 Objective 2

To develop metrology for reliable and traceable detection, identification, localisation and quantification of chemical components in the depth of organic layers as required in the manufacture of innovative devices, including novel metrological methods for 3D chemical imaging of irregular devices and complex organic-inorganic interfaces. The aim is to improve accuracy and achieve sub-50 nm lateral resolution in 3D chemical imaging by resolution enhancement resulting from the integration of topography information in the 3D reconstruction of chemical data.

### Studies of matrix effects in SIMS for improved quantification

Secondary ion mass spectrometry has been a powerful and popular analytical method for over 50 years but it has long been recognised that the analysis of non-dilute quantities would be difficult because of the strong matrix effects. These cause secondary ion signals to vary non-linearly with the composition such that quantitative analysis is generally not possible. In organic electronic devices produced by CPI, matrix effects made quantitative interpretation of depth profiles virtually impossible. During the 3DMetChemIT project, NPL conducted detailed studies of the matrix effects in organic samples were conducted, analysing a high number of secondary ions to investigate trends in the matrix effect behaviour.

First, a study was conducted of the quantification of the amount of matter when depth profiling a nominally 3.1 nm thick delta layer of the organic compound FMOC-l-pentafluorophenylalanine (FMOC) embedded in Irganox 1010. The depth profiles were made using 5 keV  $\text{Ar}_{2300}^+$  cluster ions sputtering with analysis by 25 keV  $\text{Bi}_3^+$  ions. Data for 89 negative secondary ions showed profiles whose integrated intensities as a function of depth, even when normalised to the intensity for the pure material, still varied over a factor of 12. It was shown that this variation mainly arises from matrix effects. The matrix effects were measured using separate samples with mixed layers of three intermediate compositions of the two materials. Using the measurement of the matrix effects and an appropriate model, compositional profiles from the delta layers were deduced. These gave an amount of material equivalent to  $3.22 \pm 0.07$  nm. It was concluded that the matrix terms used are a good description of the phenomenon and that SIMS profiles may be made quantitative if suitable secondary ions are available and the matrix terms are measured. In the absence of measured matrix terms, the measured quantities would be prone to large errors.

Following on from that study, a procedure was established to define the interface position in depth profiles accurately. The interface position also varies strongly with the extent of the matrix effect and so depends on the secondary ion measured. Intensity profiles at FMOC to Irganox 1010 and Irganox 1010 to FMOC interfaces were analysed for many secondary ions. These profiles show separations of the two interfaces that vary over some 10 nm depending on the secondary ion selected. Using the separate measurements of the matrix effects from mixed materials, the matrix could be removed to give consistent compositional profiles for all ions. This, however, was not straightforward but required the use of exponentially modified Gaussian function to describe the interface rather than a simple Gaussian. The average interface positions in the compositional profiles were determined to standard uncertainties of 0.19 and 0.14 nm, respectively. Alternatively, and more simply, it was shown that interface positions and profiles could be deduced from data for several secondary ions with measured matrix factors by simply extrapolating the result to zero matrix effect.

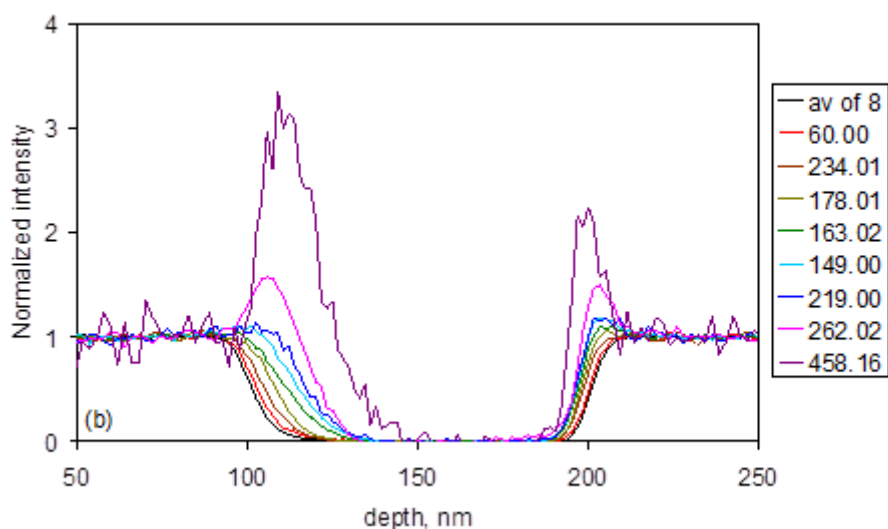


Figure 7. Normalised profiles for FMOC secondary ions. The black profile shows the average of eight ions with little matrix enhancement. The other eight profiles are for matrix terms up to the maximum value observed. The box to the right identifies the secondary ion masses in  $m/z$ .

Sets of matrix factors were measured for several binary organic systems. These showed the interplay of the effects of secondary ion velocity, fragment chemistry and the secondary ion point of origin. Matrix factors were measured for negative ions from the Irganox 1010 mixture above and for a mixture with Irganox 1098. Both positive and negative ions were measured for a mixture with  $\text{Ir}(\text{ppy})_2(\text{acac})$ . For secondary ions with  $m/z < 250$ , the matrix effect scales very approximately with  $(m/z)^{0.5}$ , supporting a dependence on the ion velocity at low mass. Low mass ions generally have low matrix factors but enhancements may still be strong even for

$m/z < 50$ . These data provide the first overall assessment of matrix factors in organic mixtures necessary for improved understanding for quantification and the precise localisation of species.

In most non-model samples, it would not be possible to measure the matrix effect. For this reason, four matrix-less methods were evaluated to determine their accuracy for establishing the interface location directly from SIMS depth profiles of organic layers. Six pure organic material interfaces were measured using many secondary ions to compare their locations from the four methods. Over all secondary ions, matrix effects cause the apparent interface positions to vary over 20 nm. The shifts in the intensity profiles on going from a layer of A into a layer of B are in the opposite direction of going from a layer of B into a layer of A, so doubling layer thickness errors. The four simple matrix-less methods are i) use of the median interface position in the intensity profiles for the 5 lightest ions, ii) extrapolation of the position for each ion to  $m/z = 0$  for ions with  $m/z < 150$ , iii) as ii) but for  $m/z < 300$  and iv) the extreme positions for all  $m/z < 100$ . Comparison with the location using the matrix terms shows their ranking, from best to worst, to be iv), iii), i) and ii) with average errors of 10 %, 12 %, 14 % and 17 % of the profile interface full widths at half maximum. Use of the most intense of the pseudo-molecular ions is very much poorer, exceeding 50 %, and should be avoided.

#### Combining SIMS and SPM for true 3D characterisation with nanoscale resolution

The above addresses quantification, and in particular interface locations, in planar structures. However, metrology is needed for 3D chemical imaging of heterogeneous systems that exhibit strong topography (e.g. structures, roughness, particles and voids etc.) and/or where large differences in erosion rates (sputter yields) exist between the constituents in the analysed volume. Whilst the imaging capability in SIMS is good, the ion beam is effectively blind to the sample topography. In the 3DMetChemIT project, this challenge was addressed by IMEC (BE) and ION-TOF using a new instrument that combines ToF-SIMS with scanning probe microscope (SPM). In the combined ToF-SIMS/SPM instrument the two types of measurements are performed iteratively by transferring the sample stage back and forth between the ToF-SIMS and SPM position where the latter brings the topographic information of the sample under investigation, without exposing the freshly-sputtered surface to air. Exploiting this information helps steering the 3D reconstruction of these systems to obtain more accurate depth scales and 3D images in heterogeneous systems.

Microstructured samples, with square holes in silicon were produced (see Objective 4 below). Briefly, the lateral dimension of the square holes as well as the pitch was between 5  $\mu\text{m}$  and 50  $\mu\text{m}$ . Organic/inorganic 3D heterogeneous microstructures were prepared by deposition of organic layers: polystyrene (PS) (spin coated) and Irganox1010 (evaporation) onto the Si templates. It would be possible to obtain depth profiles and 3D SIMS data from these heterogeneous structures but without topographic information, would not be possible to deduce the actual 3D structure only from the SIMS data. To achieve a true 3D representation, SPM images were obtained at different depths. In Figure 8 the chemical maps and the SPM images are displayed for the top layer, the two interfaces and the end of the profile. From the comparison of these measurements we can conclude that the PS was deposited thinner on the walls (signal appearing early at the PS/Si interface). Combining the topographical and chemical information, a true 3D representation was achieved.

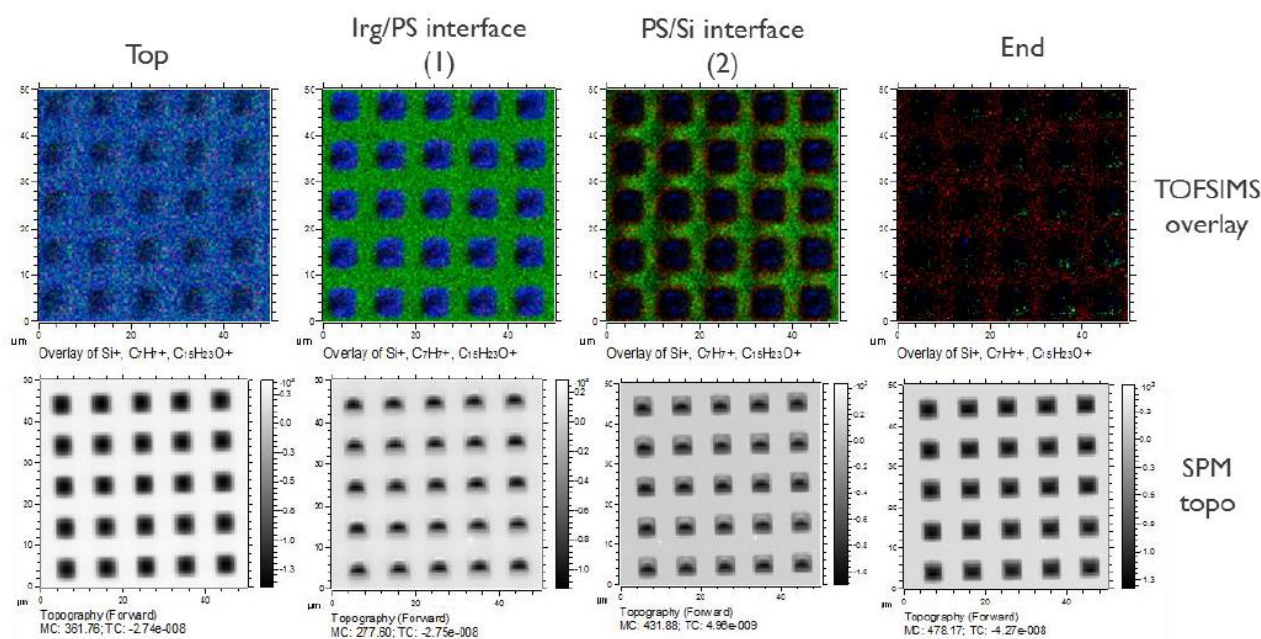


Figure 8: ToF-SIMS chemical maps and comparison with in-situ SPM measurements (topography and phase information) taken at different depths during sputtering.

In the following we describe the work carried out to achieve high resolution (3D) chemical images with ToF-SIMS. The inorganic model systems used were composed of Cu lines of varying width (50 – 500 nm) separated by SiO<sub>2</sub>. Here data will be included from two samples; 1K and 4K.

Table 1

	Sample 1K	Sample 4K
Cu line width (nm)	50 nm	60 nm
SiO <sub>2</sub> line width (nm)	50 nm	140 nm
Pitch (nm)	100 nm	200 nm

High resolution chemical surface images were recorded on sample 4K (60 nm) and 1K (50 nm). These are shown in Figure 9. The 60 nm Cu lines (sample 4K) can be clearly discerned in the Cu ToF-SIMS image (Figure 9a), validating the high lateral resolution achieved. On this sample, the image contrast could be significantly improved by pre-sputtering the surface ( $5 \times 10^{15}$  ions/cm<sup>2</sup>). The 50 nm Cu lines (sample 1K) can be likewise distinguished in the Cu ToF-SIMS image (Figure 9b) despite a significantly lower contrast when compared to the image taken on the 60 nm line sample (4K).

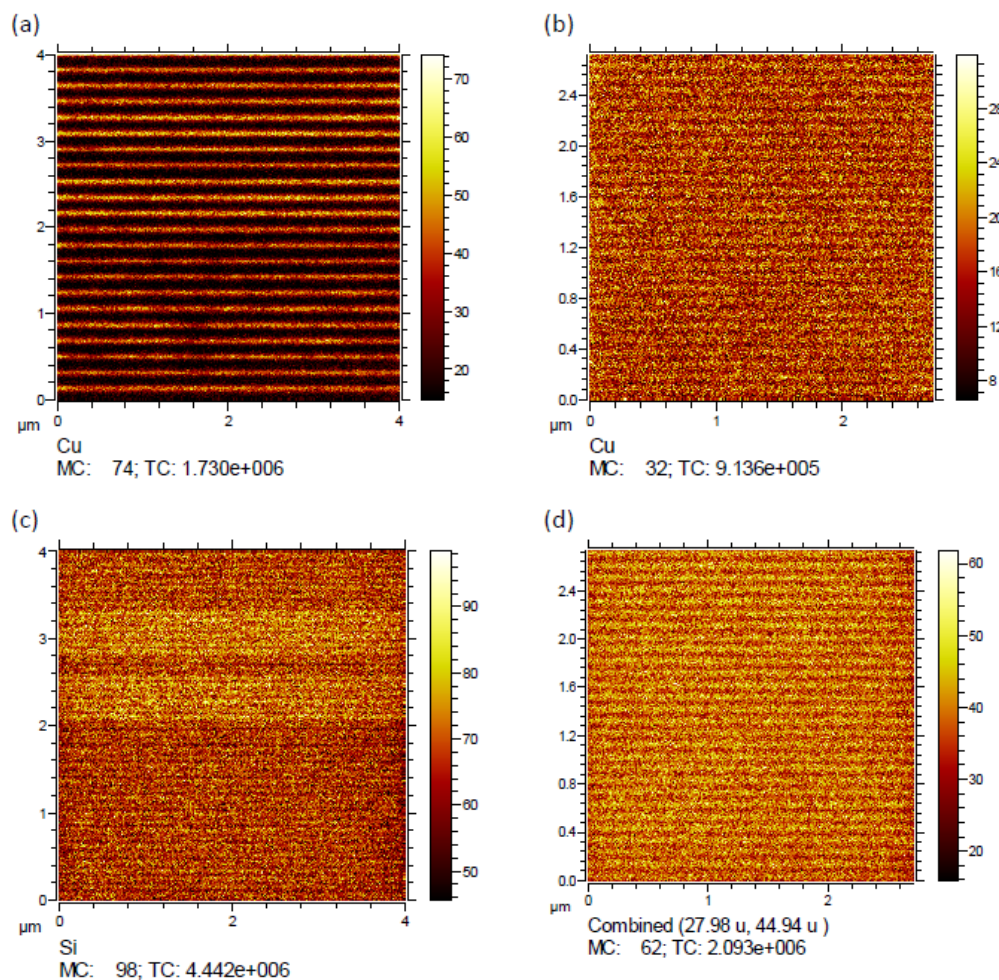


Figure 9: High resolution ToF-SIMS chemical images of 60 nm (left side) and 50 nm (right side) Cu lines separated by SiO<sub>2</sub>. The top images (a,b) show the Cu signal, the bottom images the Si (c) or the combined (Si + SiOH) signal (d). The left images on sample 4K with 60 nm line width (a,c) were recorded after presputtering with  $5 \times 10^{15}$  ions/cm<sup>2</sup>.

Chemical ToF-SIMS images of the Si as well as (Si + SiOH) signals from sample 4K and 1K are shown in Figure 9 c and d, respectively. These signals arise from the 140 nm and 50 nm wide SiO<sub>2</sub> trenches separating the 60 nm and 50 nm Cu lines, respectively.

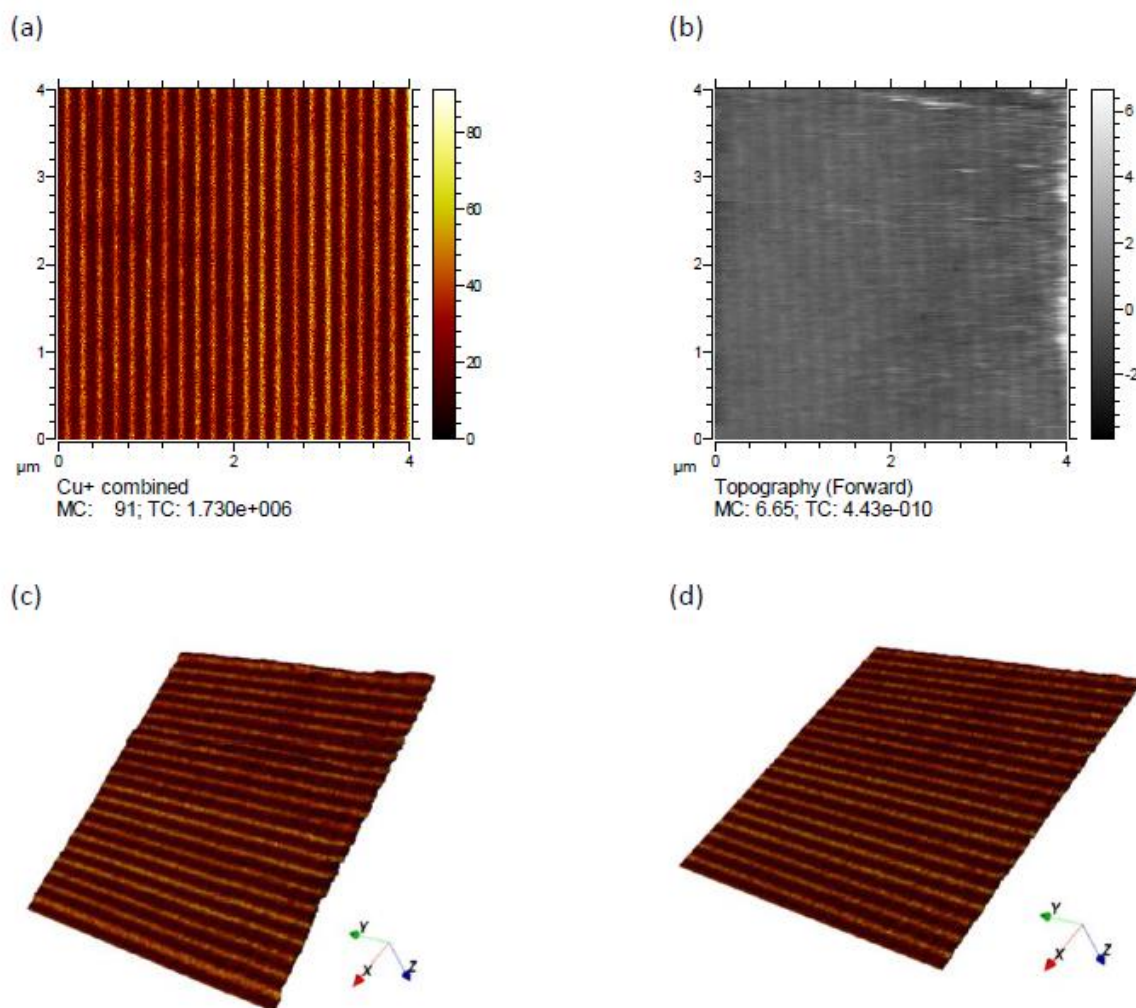


Figure 10: 3D chemical imaging of 60 nm Cu lines separated by 140 nm SiO<sub>2</sub> lines (sample 4K). The Cu ion image (a) is combined with the topography image (b) to show a realistic 3D image of the sample (c). The 3D image allows to reveal a 2 nm height difference between the Cu and SiO<sub>2</sub> lines.

The concept and feasibility of 3D chemical imaging by integrating topography information was demonstrated on the 60 nm Cu line sample (4K). The 3D reconstruction combines the Cu ion image with the topography image obtained by AFM measurements. The resulting 3D chemical image (Figure 10c) reveals that the Cu lines are approximately 2 nm higher than the SiO<sub>2</sub> lines, a result of the sample processing. The combination of ToF-SIMS and SPM has here been utilised to give corrected 3D representations with a lateral resolution of 60 nm. This is an excellent result and is considered to be satisfactory even though 50 nm was the target.

### 4.3 Objective 3

To develop a method for accurate 3D reconstruction and quantification, including the development of atomic resolution 3D elemental imaging techniques for inorganic devices and improvement of tomographic methods by the development and quantification of 3D nano structured reference materials. The objective is to obtain layer thickness/quantification accuracy better than 5 % and repeatability better than 20 % in heterogeneous systems where distortions are known to occur at present.

With the continuous scaling and simultaneous move toward complex three-dimensional (3D) semiconductor device architectures to meet future device technology needs, a corresponding shift in metrology is required.

Additionally, metrology is increasingly being required to guide novel material, device, and technology development and as such faces multiple challenges related to spatial resolution, analysable volume, speciation, and quantification. Atom probe tomography (APT) has emerged as one of the few techniques capable of dealing with the nanometric dimensions of novel devices and offers the potential to meet, in general, the above-mentioned metrology challenges. This is because APT has a theoretical lateral (0.3–0.5 nm) and depth (0.1–0.3 nm) resolution capability. However, APT is still a relatively new technique for semiconductor material analysis because its applicability within this field was only realised with the more recent advent of laser assisted APT. In the 3DMetChemIT project, IMEC (BE) investigated underlying aspects of the technique that were requiring investigation and understanding to advance the technique towards a routine and reliable metrology technique for future generation semiconductor technologies.

Atom probe tomography relies on laser assisted field evaporation one atom at the time from a nanoscale tip prepared using a FIB. 3D reconstructions are performed based on the time-of-flight for an atom to reach the detector and the position on the detector at which the atom hits which, together, provide information about the mass of the atom and the position at the tip it came from. Careful tip preparation is essential, and experimental parameters including laser energy, laser repetition rate, and tip temperature all affect the ultimate result. A study was conducted to optimise conditions for the APT analysis of GaN and  $\text{Al}_x\text{Ga}_{1-x}\text{N}$  ( $x = 0.08, 0.44, \text{ and } 0.75$ ). For GaN, conditions enabling the correct stoichiometry were found. It was found that the measured Ga and N variation as a function of the field was repeatable across different instruments, laser wavelengths, and energies/powers, thereby showing a very high level of transferability and reproducibility, key attributes for metrology applications. For  $\text{Al}_x\text{Ga}_{1-x}\text{N}$  ( $x = 0.08, 0.44, \text{ and } 0.75$ ), stoichiometric analysis conditions were not found. In this, N concentration was always underestimated. To establish the underlying cause of the N underestimation, potential loss mechanisms which include  $\text{N}_2$  sublimation,  $\text{N}_2$  neutral generation from molecular ion dissociation, and differences in the field of evaporation between the matrix elements and multihits were considered. Analysis showed that the inability to achieve stoichiometry occurs because  $\text{N}_2$  sublimation or  $\text{N}_2$  neutral generation from molecular ion dissociation is always present, unlike with GaN.

Two physical mechanisms that contribute to the quantification inaccuracy in APT analysis for the case of boron in silicon were also identified. For B in Si, the quantification accuracy was found to be more strongly determined by the B retention (in Si) as induced by the strong differences in evaporation fields, than by correlated evaporation events (multiple hits). The level of inaccuracy is linked to the electric field (and temperature) at the emitter apex and the B content may in some instances be severely (2-fold) underestimated. It was shown that the “missing” B atoms remain on the tip surface enlarging temporarily its B concentration. This build up then leads to a (slow) increase of the B-evaporation flux, ultimately creating a dynamic equilibrium whereby the retention effect is counterbalanced by an increased evaporation flux, thereby leading to the correct Si-B ratio in the evaporation flux. It is indeed expected that with increasing B concentration at the tip apex, the tip surface becomes more and more B-like, with no differential evaporation probabilities between the surface atoms and hence reducing the retention effect. In this final stationary state, the accuracy of B quantification is only limited by the loss due to multiple events, which we estimate to be around 10 %. However, the number of atoms that need to be collected before this equilibrium is reached, i.e. the width of the transient region, depends on how fast the surface becomes B-like, which is determined by B concentration in the bulk. The results showed that to reach an equilibrium state, for  $8.3\text{e}^{19} \text{ cm}^{-3}$  concentration B doped layer, it requires to evaporate several millions of atoms. As such this translates to severe profile distortions. In addition, it was found that the B retention on the emitter surface causes atomic-scale distortions of the tip shape that aberrate B ion trajectories leading to a spatially very different evaporation pattern as compared to the one of the Si atoms. This leads to an apparent excessive concentration of boron in certain locations, an artefact that becomes more pronounced at high laser energies (i.e. low field). This implies that the spatial accuracy of B-profiles is far less than usually expected from APT.

A VAMAS project to conduct an interlaboratory study on APT was prepared and initiated. Based on the input from stakeholders, the following quantities were identified to be of interest:

- film composition,
- dopant concentration,
- dopant spatial distribution,

in a ~200 nm thick, B-doped  $\text{Si}_{0.8}\text{Ge}_{0.2}$  film grown on Si(001) and capped with Si. A novel sample preparation concept was developed to reduce variance between each sample in view of sample geometry (shank angle, field of view, etc.) and sample properties (ion beam damage during sample preparation) that impact measurement results. The sample design was optimised theoretically for APT analysis, i.e. for electric field enhancement, increased field of view, sample handling and mounting (instrument compatibility). The study will be conducted in 2018-2019.

Accurate quantification in heterogeneous systems was achieved for Ge in Si where the statistical quantification uncertainty was below 10 %, the repeatability was 1.5 % and the concentration of Ge measured using APT was within 1 % of the sample composition as measured using the reference method RBS.

#### 4.4 Objective 4

*To develop a traceable method for quantifying mass depositions and element depth profiles in 3D structured nano-layered devices. Essential calibration standards, 3D nano structured reference materials, with a high control of shape and size using organic domain structures ranging from 10 nm to 100 nm, will also be developed in order to transfer traceability to online analytical instrumentation.*

This objective has three closely-linked parts. 1) The development of traceable quantification of mass depositions and elemental depth profiling based on GIXRF in 3D structured devices. 2) The development of nanostructured reference materials candidates. 3) Qualification of reference material candidates by reference-free traceable characterisation.

##### Traceable quantification of mass depositions in 3D structured devices

The work to establish traceable and quantitative characterisation of 3D micro- and nanostructured materials using grazing incidence X-ray fluorescence analysis required activities on the experimental and theoretical determination of selected atomic fundamental parameters, which are crucial for a reference-free quantification of elemental mass depositions and activities on the development of different calculation schemes for the X-ray standing wave field calculation on nanostructured samples. In Grazing Incidence XRF (GIXRF), the incident angle between X-ray beam and sample surface is varied around the critical angle for total external reflection. On flat samples, the interference between the incoming and the reflected beam results in the so called X-ray Standing Wave (XSW) field. The GIXRF technique takes advantage of this effect. Performing angular scans around the critical angle provides additional information about the depth distribution of the mass deposited on the substrate. The fluorescence signal of nanoparticles, thin layers and implantation profiles show different angular dependencies which enables elemental depth profiling by GIXRF.

X-Ray Fluorescence analysis (XRF) in general is a highly sensitive technique to determine elemental compositions and mass depositions. In particular, XRF in grazing incidence geometry allows for very low limits of detection. However, the standard quantification methods of XRF rely on reference materials or calibration standards in order to compensate for missing instrumental information. A powerful alternative is provided by the reference-free X-ray fluorescence spectrometry methodologies. By relying on radiometrically calibrated instrumentation and knowledge of the atomic fundamental parameters, no reference or calibration standards are needed for a quantitative analysis of the mass deposition of an element of interest. Depth profiling of elemental distributions using GIXRF is based on the forward calculation of the angular dependent fluorescence emission of a given depth profile for the element of interest and comparison of that response to the experimental data.

In the 3DMetChemIT project new computational tools for modelling of XSW fields in 3D structured materials were developed. Models are required for obtaining GIXRF depth profiles from structured samples but suitable modelling tools were not available before the project. One of the tools, Xraytrace, developed by the Czech Metrology Institute (CMI), is based on a voxel mesh geometry, so the material can be distributed arbitrarily within the computational space. This is an improvement over the existing literature models for X-rays' interactions with matter using geometrical optics that are designed to work only with simple objects that can be analytically defined. By using graphics cards, angular scans can be obtained in order of minutes instead of

hours, even with completely general sample geometry and tens of millions rays passed through the computational domain.

An existing computational tool, JCMWave, in which X-rays are treated as electromagnetic plane waves with a given wavelength which scatter on nanostructures, was also used to model experimental GIXRF data of a given nanostructured sample. These tools were applied to predict the shape of fluorescence vs. intensity scans as shown in the Figure below. Here, 20 nm high Cr structures topped by a  $\text{Cr}_2\text{O}_3$  layer on silicon dioxide were measured using reference-free GIXRF at the Physikalisch-Technische Bundesanstalt (PTB, DE) at 7 keV incident energy. The left hand side image shows a comparison between a modelling which is based on the effective layer approach. This approach will fail for regularly ordered structures due to additional interference effects. On the right hand side, a calculation based on Xraytrace which includes similar model parameters e.g. a modified material density, roughness and beam divergence is shown. Both approaches nicely reproduced the experimental data of this example of relatively complex experimental conditions.

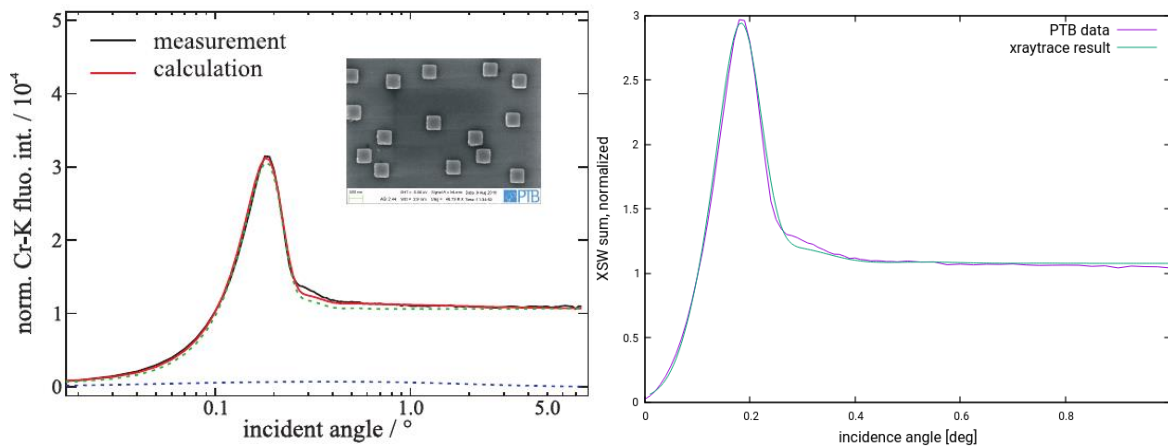


Figure 11: Dependence of fluorescence intensity on incident angle for 20 nm chromium pads, experiment and PTB modelling (left), Xraytrace simulation result (right).

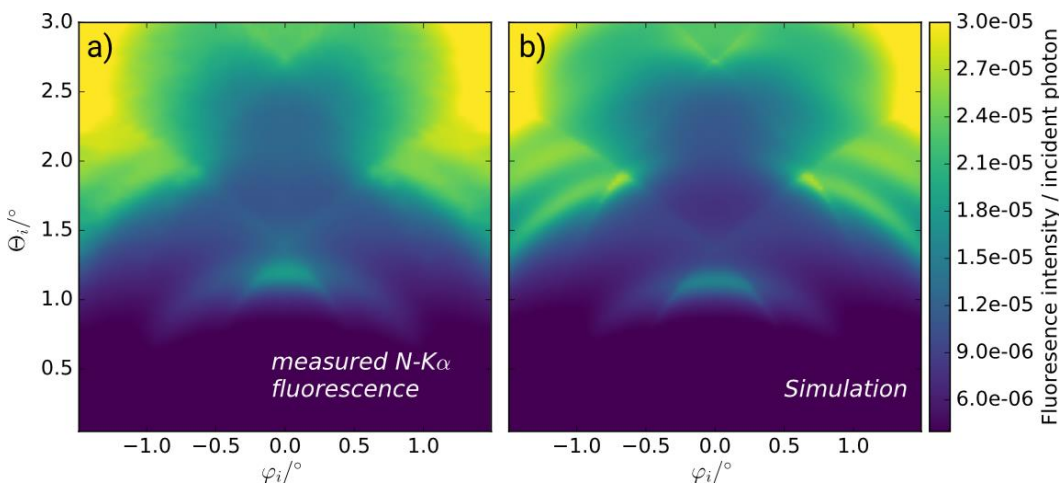


Figure 12: Comparison between the measured fluorescence intensity map (a) of the  $\text{Si}_3\text{N}_4$  grating under various incidence angles  $\theta$  and  $\varphi$  and the simulated fluorescence map (b) based on a line shape model with the best reconstruction result<sup>Error!</sup>  
Reference source not found.

Using JCMWave based FEM calculations of the XSW, a characterisation was performed on nanoscale  $\text{Si}_3\text{N}_4$  grating structures. For this system, the overall agreement between experimental data and the calculation result is very good for the full angular ranges.

Fundamental parameters are behind any quantification using XRF. In the project, K-shell fundamental parameters of Ni were experimentally determined independently at X-ray facilities at the French Alternative Energies and Atomic Energy Commission (CEA) and at PTB. Both the transmission and the emitted fluorescence intensities for Ni  $K_{\alpha}$  and Ni  $K_{\beta}$  fluorescence radiation were measured for various monochromatic incident photon energies around the K attenuation edge of Ni. Together with the other known instrumental and experimental parameters, e.g. the solid angle of detection and the incident photon flux, the fluorescence production cross sections for Ni  $K_{\alpha}$  and Ni  $K_{\beta}$  of the used thin foil could be quantified, and the Ni-K fluorescence yield was derived from this data. The resulting value is shown in comparison to already published results in Table 12. The main contributors to the stated uncertainty budget are the attenuation correction factor and the determination of the photoelectric cross sections.

Table 1: Experimental and theoretical K-shell FY results for Ni. Results are compared with most common literature values. Experimental uncertainties are indicated within brackets.

Data source	$\omega_K$
PTB result	0.410(14)
CEA result	0.421(7)
UNL result (3d8 4s2)	0.417
UNL result (3d9 4s)	0.415
Krause	0.412(21)
Cullen	0.401

Fundamental parameters were also determined through a theoretical approach by the New University of Lisbon (FCT-UNL, PT). Specifically, the fluorescence and Coster-Kronig yields were calculated using the radiative and radiation-less transition rates calculated within the Dirac-Fock framework. Calculations were performed for the K- and L-shells of Ni, and the results were compared with the recent experimental results, as well as results from the literature. The first thing that stands out from the results is that for the K-shell, there is an excellent agreement between the theoretical results and the experimental results above, as well as with most results from the literature. The resulting values for the Ni-K shell fluorescence yields for the two experimental determinations from PTB and CEA as well as for the theoretically calculated values from UNL are shown in Table 11. A good agreement both with respect to commonly used literature values and the different determined values from this project was found. In addition, the uncertainty of the Ni-K-shell yield is lower than for the often used Krause value, which allows for reduced quantification uncertainties for Ni using the K-shell fluorescence.

Following the determination of the parameters for Ni, fundamental parameters were also determined for the L-shell of Sn. A good agreement between one set of experimental FPs and calculated values was found, while the other set of experimentally determined FPs deviated slightly. Further validation of the values would be necessary to clarify the differences between the two experimental data sets.

The knowledge of all relevant instrumental and atomic fundamental parameters allows for calculating mass depositions of an element within a unit area. This was performed at CEA and PTB from the experimental data for the two samples where elemental mass depositions for Ga and Zn were quantified. For both elements, an excellent agreement within the stated uncertainties was found between the results from the two facilities.

The work carried out enabled traceable quantitative characterisation of nanoscale samples including 2- and 3D nanostructures using reference-free GIXRF analysis. Such a characterisation was not possible before due to the fact, that the additional effects when performing GIXRF analysis of regularly ordered nanostructured samples could not be modelled. The calculation of the XSW is much more complex on such samples and is now possible and successfully demonstrated by the results presented in the present deliverable document and the publications related to these activities. This developed knowledge enabled the reference-free GIXRF based characterisation of the nanostructured calibration sample candidates below.

### 3D micro- and nano-structured systems for calibration standards.

Three different organic/inorganic reference materials were fabricated incorporating silicon, polystyrene and Irganox 1010 in three different length scales.

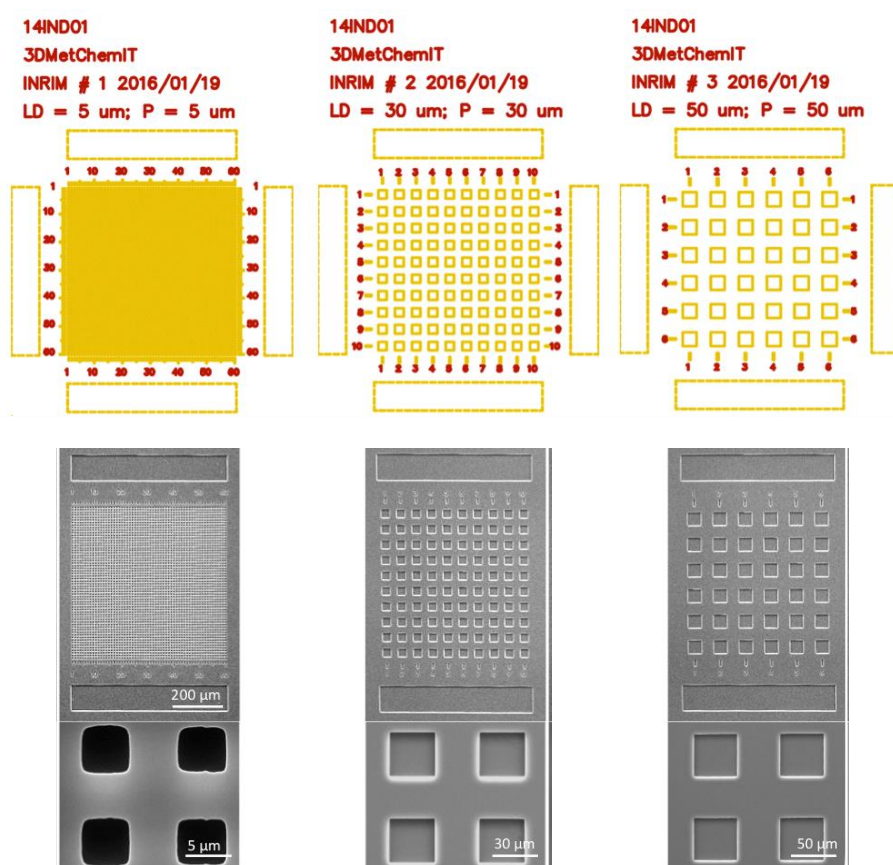


Figure 13: 3D model systems at the microscale developed and characterised in 3DMetChemIT. From left to right: Model#1, Model#2, and Model#3. P: pitch in  $\mu\text{m}$ , LD: Lateral Dimension in  $\mu\text{m}$ .

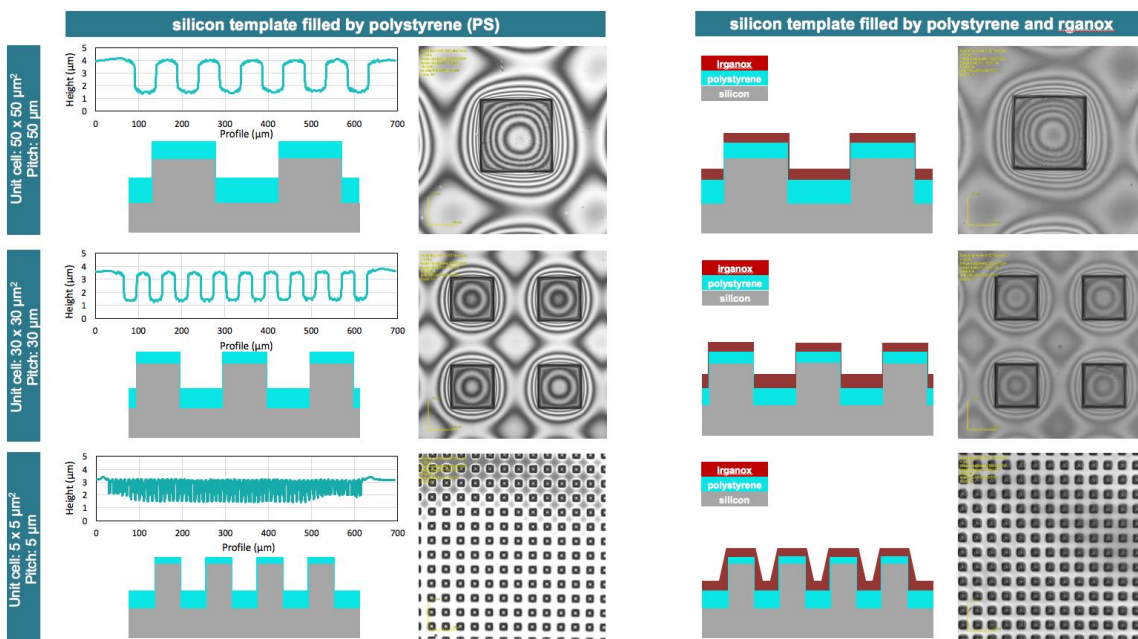
Micro structured templates were fabricated by INRIM, the Italian National Metrology Institute, in silicon using optical lithography (laser writer), and then pattern-transfer to the silicon substrate was performed by reactive ion etching (RIE) using the Bosch process ( $\text{SF}_6/\text{C}_4\text{F}_8$ ). Each template had a square shape unit cell ( $5 \times 5$ ,  $30 \times 30$  or  $50 \times 50 \mu\text{m}^2$ ) with a pitch equal to the square's side and depth (Z-dimension) of  $2.3 \mu\text{m}$ . The total micro structured area was about  $600 \times 600 \mu\text{m}^2$  for all three templates. Dimensional characterisation was performed using both SEM and optical profilometer. Finally, a certification on dimensional characterisation (including uncertainty budget) was issued for each template model. One sample for each feature size was filled with PS by spin coating, (PS concentration in toluene:  $133 \text{ mg/ml}$ ) and cleaned by  $\text{O}_2$  plasma. From profilometric analysis the final polystyrene thickness at the bottom of the structures was about  $0.9 \mu\text{m}$ . One sample for each feature size was employed as sacrificial samples and filled with PS and analysed by SEM after cross-section. The thermal stability of the materials at different size scale was assessed. The thermal stability of  $1 \mu\text{m}$  thick film was found to be equal to the bulk. Finally, a  $1 \mu\text{m}$  layer of Irganox 1010 was deposited on the sample by NPL. The completed sample was imaged using a laser confocal microscope.

Dimensional characterisation of silicon templates was carried out by the Length metrology department of INRIM using a calibrated Optical profilometer. The average area and depth (z-direction) of structures were measured for the template model 1 and 2 ( $50 \times 50$  and  $30 \times 30 \mu\text{m}^2$ ), while in the case of template model 3 ( $5 \times 5 \mu\text{m}^2$ ), only the depth of two guide trenches, on the top and the bottom of micro-structured area, were measured. The obtained results with the calculated standard uncertainty is reported in the table below. Finally, a certification on dimensional characterisation of reference templates was issued by INRIM as well.

Table 3: Dimensional characterisation of nanoscale templates.

Sample	A5-1		A30-2		A50-3	
		uncertainty U		U		U
Average area of unit cell / $\mu\text{m}^2$	32,1	2,5	972	29	2636	53
Average depth of unit cell (z-direction) / $\mu\text{m}$	-----	-----	2,353	0,033	2,371	0,042
Depth (z-direction) on right trench / $\mu\text{m}$	2,338	0,011	-----	-----	-----	-----
Depth (z-direction) on left trench / $\mu\text{m}$	2,331	0,011	-----	-----	-----	-----

Morphological characterisation of filled templates was performed using an optical profilometer. In particular, the relative depth of microstructures was measured after each filling steps (PS or Irganox). The results are reported in Figure 14. A gradient in the thickness of PS film, for all three type of samples, was observed on mesa between two successive structures (Figure 14, left side). Nevertheless, this gradient was negligible with respect to the topography of the PS film (Figure 14, PS profile).



	Model 1	Model 2	Model 3	
	50 x 50 $\mu\text{m}$	30 x 30 $\mu\text{m}$	5 x 5 $\mu\text{m}$	
Average depth of silicon template(z-direction) / $\mu\text{m}$	2.335	2,353	2,371	
Average relative depth microstructures filled with PS / $\mu\text{m}$	2.5	2.5	1.5	
Average relative depth of microstructures, filled with PS + irganox / $\mu\text{m}$	2.5	2.5	1.5	

Figure 14: Morphological characterisation of filled templates, using optical profilometer.

To create nanoscale structures, three different organic/inorganic reference materials were fabricated based on silicon template and polystyrene thin film deposition. The appropriate random copolymer was prepared by University of Eastern Piedmont (UPO, IT) in order to obtain the neutralisation of the substrate surface. In particular, two surface modifiers were prepared with low molar mass to improve the pattern transfer fidelity and to obtain the perpendicular orientation of the nano-structures. Nano structured templates were fabricated using di-block copolymer (DBC) self-assembly as lithographic masks and the pattern transfer to the silicon substrate has been performed by reactive ion etching (RIE) using cryogenic mixing mode of  $\text{SF}_6/\text{O}_2$ . Three asymmetric PS-b-PMMA DBCs with different molar mass ( $M_n = 54, 67, 82 \text{ Kg/mol}$ ), also prepared by UPO, were selected

for fabrication of nano structured templates. The Institute for Microelectronics and Microsystems at the National Research Council of Italy (CNR) optimised the processing of the polymer to form nanostructures with the following feature dimensions:

B54 (D=13, P=28, Depth=16 nm)

B67 (D=17, P=35, Depth 30 nm)

B82 (D=19, P=43, Depth=30 nm)

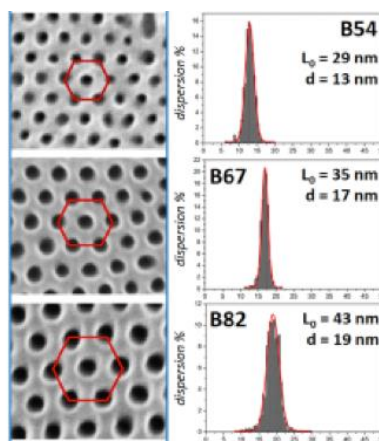


Figure 15: The resulting polymeric masks of the selected BCPs.

Pattern transfer to the underlying substrate by RIE was optimised for each DBC. AFM and SEM analysis were used to characterise the surface morphology of the patterned silicon substrates, providing information about periodicity and pore diameter. Concurrently XRR was used to validate an ellipsometric model that allows determining the average depth of the pores. XPS analysis was used to probe the electronic structure of the nanoporous inorganic template. The filling procedure has been attempted by spin-coating on top of the three nanostructures of a PS film (molecular weight: 30 kg/mol) of about 15 nm thick. Then a thermal treatment in RTP at 250 °C for 10 min was performed. The thermal stability of thin films is higher than for the bulk and increases as the thickness decreases. Thermal characterisation was carried out using a TGA-GC-MS apparatus.

The pore depth was measured by means of two independent techniques, in order to validate the result. In table 4 we report the values obtained from spectroscopic ellipsometry and from X-Ray Reflectivity (XRR). Both the techniques acquired indirectly the thickness of the porous layer, passing through a data fit. The pore depth for holey Ge and holey SiGe is validated within 1-3 nm, whereas for holey Si a difference of 5-6 nm is shown. The discrepancy can be explained by the high roughness of the samples, probably due to an excessive etching time (120 s), for which the RIE process could degrade the polystyrene mask and consequently etch the whole silicon surface.

This effect was investigated in more details performing a systematic study of pattern transfer to silicon as function of the pore diameter of the self-assembled template and thickness of the polymeric mask [3].

The nanoscale structures were filled with polystyrene by spin coating from a toluene solution followed by a thermal annealing in a Rapid Thermal Processing (RTP) apparatus at UPO. Three different standard polystyrene samples, with molar mass of 2150, 7000 and 11300 g/mol were employed. The polymers were dissolved in toluene at a concentration of 6.0 mg/ml and the solutions were spin-coated onto the substrates for 30 s at 2000 rpm. Before polymer deposition the substrates were cleaned by sonication in toluene for 900 s and then dried under N<sub>2</sub> flow. The samples were then annealed using a rapid thermal processing (RTP) apparatus at 250 °C for 900 s in a N<sub>2</sub> atmosphere.

Table 4: Morphological parameters of polymer masks and corresponding holey semiconductors (HS). The columns show the holes diameter ( $d$ ), the hole-to-hole distance ( $L_0$ ) and the pore depth ( $h$ ).  $H$  values were measured using ellipsometry ( $h_e$ ) and XRR ( $h_x$ ). Each row shows the parameters related to a specific pair semiconductor - BCP molecular weight  $M_n$  [g/mol].

Template	Substrate	$d$ [nm]	$L_0$ [nm]	$h_e$ [nm]	$h_x$ [nm]
B54	Si	$12 \pm 1$	$29 \pm 1$	12	18
B67	Si	$24 \pm 1$	$35 \pm 1$	23	29
B82	Si	$22 \pm 1$	$43 \pm 1$	27	-
B67	Ge	$21 \pm 1$	$36 \pm 1$	28	25
B82	Ge	$22 \pm 1$	$43 \pm 1$	22	25
B67	SiGe	$18 \pm 1$	$36 \pm 1$	29	19
B82	SiGe	$21 \pm 1$	$41 \pm 1$	21	23

#### Establishing traceable measurements

With the use of PTB's reference free GIXRF technique, a traceable quantitative characterisation of the various nanoscale calibration samples was performed in order to qualify them and to establish a chemical traceability of the 3D characterisation techniques used in the project. In addition, several initial comparison experiments with the techniques ToF-SIMS and APT were. The results obtained were promising as they showed good agreement in terms of the quantified amount of the respective material.

With the development of new micro- and nano-structured reference material prototypes and the development of a method for the traceable characterisation of these, the project fully met Objective 4.

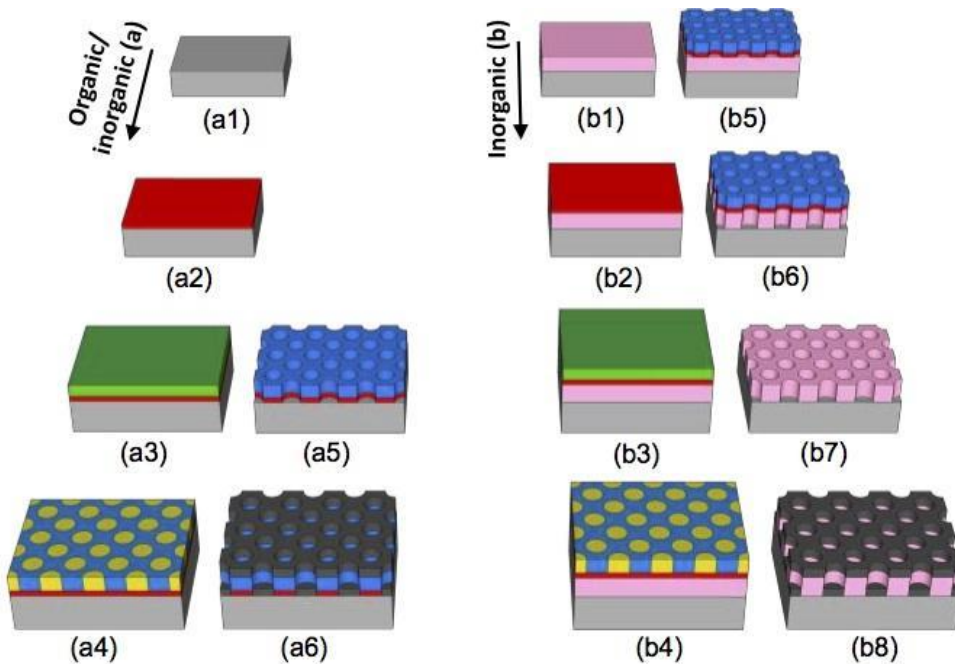


Figure 16: Sketch of preparation procedure for organic/inorganic (a) and inorganic (b) samples: (a1), (b1) Cleaning and surface functionalisation of Si or SiO<sub>2</sub> substrate. (a2), (b2) Deposition and grafting of random copolymer (RCP). (a3), (b3) Deposition of block copolymer. (a4), (b4) Phase separation between PS and PMMA in vertical aligned cylindrical configuration. (a5), (b5) Selective removal of PMMA with respect to PS and removal of RCP thin layer from bottom of the cylindrical shaped holes. (b6) Pattern transfer to the SiO<sub>2</sub> substrate. (b7) Removal of the organic residuals in Piranha solution. (a6), (b8) Deposition of Al layer (over full surface area). Colour code in the figure: RCP (red), DBC (green), PMMA (yellow), PS (blue), Al (dark grey), SiO<sub>2</sub> (pink) and Si (silver).

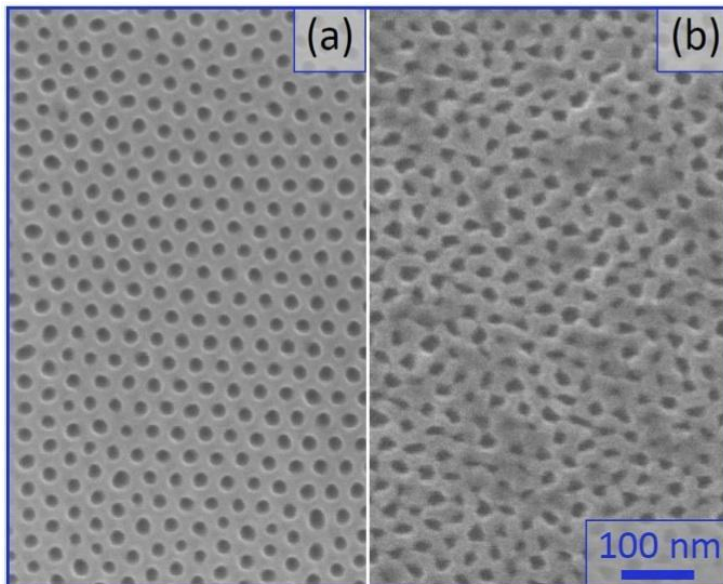


Figure 17: SEM image of DBC mask (a). Nanostructured Al film after deposition of Al (b).

## 5 Impact

A total of 11 papers have been published in peer-reviewed journals and are open access, and a further five papers have been submitted or are in preparation. Additionally, 106 conference presentations and posters were presented over the lifetime of the project. There have also been a number of conferences, training sessions and workshops to aid the uptake of the work completed in this project.

ION-TOF have held various workshops such as the 11th DACH FIB Workshop exploring novel FIB source concepts, FIB based analytics and FIB based applications in different research fields. A workshop organised by the project consortium (EMRS/ALTECH) has also aided the uptake of methods developed in the 3DMetChemIT project, with many partners taking part to discuss techniques and disseminate results. The 79th IUVSTA Workshop, reviewing 3D Chemical imaging and organised by NPL, INRIM and IMEC was organised in June 2017 where over 26 people across a mixed audience (industry, academia etc.) participated.

Currently there are further plans for another training workshop as a satellite event to SIMS Europe in 2019 in Germany, to discuss methods developed in this projects.

### *Impact on relevant standards*

In ISO TC 201 (Surface Chemical Analysis), the project has provided input to a new work item proposal on measurement of the sputtering yield in gas cluster ion sputter depth profiling of organic materials. This is the first formal step towards the development of an international standard for measuring this important parameter which will help laboratories measure the depth of interfaces in sputter depth profiles.

NPL has had input into a draft documentary standard for the interactions standards development organisation of TC 201 (surface chemical analysis) committee of the SC6 (secondary ion mass spectrometry) subcommittee in September 2017.

### *Impact on industrial and other user communities*

The project advanced the measurement capability and provided the essential metrology for spatially resolved chemical analysis. This will have direct impact across a broad range of industry sectors, all with the need for 3D chemical metrology. These include, but are not limited to, industries dealing with semiconductors, carbon-based electronics (organic electronics, graphene), medical devices, advance manufactured multi-layered films and additive manufacturing. The metrology output is, in the first instance, targeted at these industries and measurement service providers addressing industry issues.

X-ray spectrometry fundamental parameters for Ni were determined in the project. The fundamental parameters are required for accurate quantification with x-ray fluorescence. These new values were taken up by two x-ray fluorescence instrumentation vendors.

SIMS analysis is commonly used for identification and imaging of contaminants resulting from materials processing and affecting device or material performance. A more than 10-fold improvement in mass resolution in SIMS (from 10 000-15 000 to > 150 000) significantly improves the reliability of chemical identification with immediate impact for the end users that need to identify contaminants to pinpoint processing issues. This capability by autumn 2018 will be available at three partner organisations.

### *Impact on the metrology and scientific communities*

The fundamental parameters determined for Ni will become widely available and improve accuracy in x-ray fluorescence spectrometry, a widely used technique in materials analysis.

### *Longer-term economic, social and environmental impacts*

The improved measurement capability is projected to underpin development and manufacture in a range of industries including the semiconductor, steel and energy storage industries where analysts are faced with challenges to measure the chemical composition of inorganic devices or heterogeneous systems containing organic/inorganic layers and interfaces. This can have a great effect on performance of a product and therefore lifetime. By allowing for accurate measurements of these layers, it may be possible to identify defects more readily and remove materials that can have a detrimental effect on product lifetime or efficiency.

## 6 List of publications

1. S. Surana, T. Conard, C. Fleischmann, J. G. Tait, J. P. Bastos, E. Voroshazi, R. Havelund, M. Turbiez, P. Louette, A. Felten, C. Poleunis, A. Delcorte, W. Vandervorst, *Understanding the physico-chemical aspects in the depth profiling of polymer:fullerene layers*, J. Phys. Chem. C, 2016, 120, 28074.
2. M. Tiddia, G. Mula, E. Sechi, A. Vacca, E. Cara, N. De Leo, M. Fretto, L. Boarino, *4-Nitrobenzene grafted in porous silicon: an application to optical lithograph*. Nanoscale Research Letters, 2016 11, 436.
3. M. Dialameh, F. Ferrarese Lupi, D. Imbraguglio, F. Zanenga, A. Lamperti, D. Martella, G. Seguini, M. Perego, N. De Leo, L. Boarino, *Influence of the Block Copolymer feature size on pattern transfer into silicon*, Nanotechnology, 2017, 28, 404001.
4. P. Seah, R. Havelund, I. S. Gilmore, *SIMS of Delta Layers in Organic Materials: Amount of Substance, Secondary Ion Species, Matrix Effects, and Anomalous Structures in Argon Gas Cluster Depth Profiles*, J. Phys. Chem. C, 2016, 120, 26328.
5. R. Havelund, M. P. Seah, M. Tiddia, I. S. Gilmore, *SIMS of Organic Materials – Interface Location in Argon Gas Cluster Depth Profiles Using Negative Secondary Ions*, J. Am. Soc. Mass Spectrom., 2018, 29, 774.
6. M. Guerra, J. M. Sampaio, F. Parente, P. Indelicato, P. Honicke, M. Muller, B. Beckhoff, J. P. Marques, J. P. Santos, *Theoretical and experimental determination of K- and L-shell X-ray relaxation parameters in Ni*, Phys. Rev. A, 2018, 97, 42501.
7. F. Scholze, J. Probst, J. Eilbracht, Y. Kayser, P. Honicke, V. Soltwisch, B. Beckhoff, *Element sensitive reconstruction of nanostructured surfaces with finite elements and grazing incidence soft X-ray fluorescence*, Nanoscale, 2018, 10, 6177.
8. W. Vandervorst, P. van der Heide, L. Arnoldi, M. Zhao, C. Fleischmann, D. Melkonyan, R. J. H. Morris, R. Cuduvally, *Toward accurate composition analysis of GaN and AlGaN using atom probe tomography*, J. Vac. Sci. Technol. B, 2018, 36, 03F130.
9. B. Pivac, M. Perego, G. Seguini, P. Dubček, W. Vandervorst, C. Fleischmann, T. Weimann, Y. Kayser, B. Beckhoff, P. Honicke, F. Ferrarese Lupi, M. Dialameh, N. De Leo, L. Boarino, *Development and Synchrotron-Based Characterization of Al and Cr Nanostructures as Potential Calibration Samples for 3D Analytical Techniques*, Phys. Status Solidi A, 2018, 215, 1700866.
10. T. Conard, C. Fleischmann, R. Havelund, A. Fanquet, C. Poleunis, A. Delcorte, W. Vandervorst, *Inorganic material profiling using Ar<sub>n</sub><sup>+</sup> cluster: Can we achieve high quality profiles?*, Applied Surface Science, 2018, 444, 633.
11. M. K. Passarelli, A. Pirkl, R. Moellers, D. Grinfeld, F. Kollmer, C. F. Newman, P. S. Marshall, H. Arlinghaus, R. Havelund, M. R. Alexander, A. West, S. Horning, E. Niehuis, A. Makarov, C. T. Dollery, I. S. Gilmore, *The 3D OrbiSIMS—label-free metabolic imaging with subcellular lateral resolution and high mass-resolving power*, Nature Methods, 2017, 14, 1175. Full text available via <http://europepmc.org/abstract/MED/29131162>.